Applied Nanoscience (2021) 11:1617–1635
https://doi.org/10.1007/s13204-021-01817-4

ORIGINAL ARTICLE

An in-depth examination of opto-electrical properties of In-Yb_2O_3 thin films and fabricated Al/In-Yb_2O_3/p-Si (MIS) hetero junction diodes

K. S. Mohan[1] · A. Panneerselvam[2] · J. Chandrasekaran[3] · R. Marnadu[3] · Mohd. Shkir[4]

Received: 31 December 2020 / Accepted: 22 March 2021 / Published online: 21 April 2021
© King Abdulaziz City for Science and Technology 2021

Abstract

In the proposed work, the thin films have been effectively synthesized by doping the post-transition metal with rare earth metal (In-Yb_2O_3) on a large scale using a low-cost jet nebulizer spray pyrolysis technique at different indium (In) doping concentration (0, 1.5, 2.5, 3.5, and 4.5 wt %) with optimized substrate temperature 550 °C. The structural, morphological and opto-electrical properties are investigated using various characterization techniques. Here, the high-quality single-phase cubic structure film was observed by X-ray diffraction (XRD) analysis. The field emission scanning electron microscope (FESEM) image reveals the change in morphology with indium (In) concentration in Yb_2O_3 thin films. The elemental composition study approves the presence of Yb, In and O. The transmittance, optical indirect energy gap of In-Yb_2O_3 films have been analyzed by UV–Vis spectra. DC electrical analysis records an improved conductivity and reduced average activation energy for higher doping content of In-Yb_2O_3 thin films. Notably, all the diodes shows positive photo conducting properties. Specifically, when the Al/In-Yb_2O_3/p-Si Schottky barrier diode fabricated with higher doping concentration such as 4.5 wt. % produces the minimum ideality factor (1.791), maximum barrier height (0.692 eV) and higher photosensitive diodes.

Keywords Rare earth metals · Yb_2O_3 · Jet nebulizer spray pyrolisis method · MIS Schottky diode · Optical and electrical properties

Introduction

In the modern scenario, the attractive and very effective optoelectronic and photo detector devices have a wide focus by the researchers. Especially, most favored and low power consumption devices like Metal Insulator Semiconductor (MIS), Schottky Barrier Diodes (SBD), and photodiodes contain excellent electrical behaviors than the other layered devices such as Metal–Insulator-Metal (MIM), Metal-Polymer-Semiconductor (MPS), and Metal–Oxide–Semiconductor (MOS) (Khanfar et al. 2017; Scarel et al. 2006; Riazimehr et al. 2017). The unique features of Schottky barrier diodes are low forward voltage values for the diodes between 0.2 and 0.3 V, a small amount of stored change that can be used for high-speed switching applications and high operating frequency (Bartolomeo et al. 2019; Balaji et al. 2020a). Besides, Schottky diodes have an active role in different applications such as radiofrequency generator, biological sensors, optical communication system and microelectronic devices because of their tunable characteristics like stability and opto-electrical properties (Casalino et al. 2017; Qian et al. 2017; Terasaki et al. 2009).

Fabrication of superior metal insulator semiconductor (MIS) system is essential, since the electrical behavior of SBDs sturdily reliant to MIS interface quality. The performance of MIS devices depends on multi-factors, including the existence of interfacial layer at metal–semiconductor interface and its thickness. Interface layer having significant role in several electronic devices and the outcome from this layer on SBDs can be merely modernized by

✉ A. Panneerselvam
panneer.phy@gmail.com

1 Department of Physics, Nandha Engineering College (Autonomous), Erode 638 052, Tamil Nadu, India

2 Department of Physics, Vivekanandha College of Engineering for Women (Autonomous), Elayampalayam, Tiruchengode, Namakkal 637 205, Tamil Nadu, India

3 Department of Physics, Sri Ramakrishna Mission Vidyalaya College of Arts and Science (Autonomous), Coimbatore 641 020, Tamil Nadu, India

4 Advanced Functional Materials & Optoelectronics Laboratory, Department of Physics, College of Science, King Khalid University, Abha 61413, Saudi Arabia

suitable organic, rare metals/metal oxides and polymers (Munikrishna Reddy et al. 2015). Advanced rectification nature of MIS is achievable through inserting a layer of insulating material compared to metal semiconductor (MS) device. Hence, a selection of appropriate material layer and its thickness is a key factor for MIS as it affects the barrier height (Φ_B), ideality factor (n), and sheet resistance (R_S) of the device. Fascinatingly, the MIS device becomes more popular in variation to other types of SBDs because of their multifaceted application (Kahraman et al. 2020; Prnová et al. 2014). In past few decades, the rare earth materials are having great attention in optoelectronic devices, such as photo diodes, photo detector and microelectronics. Especially, various rare earth materials used in MIS structured SBDs such as ytterbium (Yb), samarium (Sm), neodymium (Nd), erbium (Er) and Cerium (Ce) are important materials having good transparency, insulating behavior and semiconducting nature. Furthermore, they are used as layer in different devices like MIS diodes, MOS capacitors and transistors due to their high-dielectric behaviors (Zargouni et al. 2020a; Puri et al. 2019; Jyothi et al. 2016). Among these insulating layers, Yb_2O_3 is a multifunctional one, that displays extensive range of novel characteristics like phase conversion, wide energy gap (> 4.9 eV), robust absorption of light, higher crystallinity, better dielectric constant, thermal stability at higher temperature and luminescence. Yb_2O_3 material with unique property is suitable for MIS structure interface layer. The post-transition metals are fascinating aspirants as doping element due to metal ions addition, which can easily incorporate to host ions that may enhance the way of operation and characteristics of diode that will result in advancing the device performance. Especially, Cu, In, Cd, Sn and Bi metals are n-type semiconductors and ultimate cationic addition to Yb_2O_3 films because of ionic radii of In^{3+} is quite similar to Yb^{3+} ions, which might be easily incorporated to host ions. Indium can be used as a transparent conductive oxide material in optoelectronic device, including light emitting diodes and photo detectors due to enhance optical properties (Narmada and Kathirvel 2019; Rajagopal Reddy et al. 2013).

Many researchers have made an effort to inveterate the electrical nature of p-Si Schottky barrier diodes (SBDs) via different metallization schemes, and its usage in sensing and optoelectronics (Luongo et al. 2018; Bartolomeo January 2016). Barrier height (Φ_B) values are calculated from I-V measurements for Cu/Sn-WO_3/p-Si, Au/Zn-Au/p-InP, Cu/MoO_3-ZrO_2/p-Si that are ranging from 0.69 to 0.66, 0.58–0.72, 0.585–0.66 eV, respectively (Raj et al. 2020; Asubay 2011; Vivek et al. 2019a). Thangaraju et. al. inspected electrical characteristics of n-SnS_2/p-Si with respect to increasing doping level and documented a high ideality factor for MIS diodes (Thangaraju et al. 2020). However, the electrical conductivity of the rare earth metals is good when compared to abovementioned results. The huge Φ_B, minimal leakage current and low ideality factor produced by the good quality schottky contacts that can lead to improve the device activities. Furthermore, many researchers have developed SBDs through GaN, GaAs, InP and Si as dissimilar substrates (Buyukbas-Ulusan et al. 2019; Sonmezoglu and Akın 2012; Chen et al. 2016). These reports reveal that the indium (In) doped Yb_2O_3 (In-Yb_2O_3) films and the development of Al/In-Yb_2O_3/p-Si Schottky diode are not documented till date. Hence, this present work is an attempt to fabricate and study the Al/In-Yb_2O_3/p-Si Schottky diode. As Yb (2.60 eV) has low work functions and unfavorable configuration of energy gap that is predictable to generate higher Φ_B that will provide superior rectifying behavior for p-Si. Among the available techniques, the jet nebulizer spray pyrolysis (JNSP) process is facilely used to cast nano structured thin films. Also, Jet nebulizer spray pyrolysis method procedure possesses several advantages like high-homogeneity, cost-effective, concentration of spray solution and wide area coating (Suresh et al. 2014; Balaji et al. 2016; Vivek et al. 2020).

In this investigation, we prepare Indium doped Ytterbium oxide (In-Yb_2O_3) thin films on glass substrates with various indium (In) doping concentration like 1.5, 2.5, 3.5 and 4.5 wt. % with optimized temperature 550^0C. The influence of indium concentration on structure, morphological and opto-electrical characteristics of Yb_2O_3 films is conferred. Further, the major goal of authors is to develop the Al/In-Yb_2O_3/p-Si Schottky diodes using insulating In-Yb_2O_3 film layer among Al/p-Si interfaces. Several important parameters like n, Φ_B, photosensitivity (Ps) and saturation current (I_0) of the diode are extracted using I-V characteristics for different doping concentrations of indium (In).

Experimental methods

In-Yb_2O_3 thin films fabrication

The analytical grade of rare earth materials Ytterbium (III) chloride hexahydrate ($YbCl_3.6H_2O$) and Indium chloride ($InCl_3$) of 99.9% purity were acquired through Sigma-Aldrich. Ytterbium (III) chloride hexahydrate and Indium chloride are used as the source of ytterbium and indium materials are casted on hot IPA and acetone cleaned substrate through JNSP route via carrier gas. For undoped Yb_2O_3, thin film preparation process of 0.1 mol of $YbCl_3.6H_2O$ is liquified in 10 ml de-ionized water and 45 min. stirring is done at 300 K via magnetic stirrer. Likewise, 0.1 mol of $InCl_3$ was readied. These pure solutions are poured into doped solutions with diverse concentration of 1.5, 2.5, 3.5 and 4.5 wt. %. The prepared solutions are deposited on substrates at optimized temperature 550 °C using jet nebulizer spray pyrolysis route. Size of all substrates is 2×2.5 cm^2

for preparing undoped and Indium doped Yb_2O_3 films via effective method.

Development of Al/ In-Yb_2O_3/p-Si schottky barrier diodes

The Al/ In-Yb_2O_3/p-Si (MIS) diodes are cast on p-Si. Prior to cast the diode, the wafer is cleaned well and it is inserted in 3:1 ratio of $H_2SO_4 + H_2O_2$. In favor to evade undesirable layer of oxide from Si wafer, the layer of In-Yb_2O_3 is deposited by JNSP. The Aluminum (Al) as metal contact is coated on In-Yb_2O_3/p-Si layer via dc magnetron sputtering technique through a shadow mask with the standard pressure 6 mbar. The fabricated MIS diode is dried in air for 12 hrs inside clean chamber. The Ag paste is employed on either side of MIS diodes and dried at 300 K for 5–6 h. The structure of prepared MIS diodes is publicized in Fig. 1.

Characterization techniques

First, the quality of the prepared pure Yb_2O_3 and In-Yb_2O_3 thin films are analyzed by Rigaku Miniflex-II ($CuK\alpha_1$ radiation with $\lambda = 1.5418$ Å) with the diffraction range of $(10 - 80^{\circ})$. Stylus Profilometer detector (model: SJ-30) is used to measure the thickness of the film. Atomic force microscopy (model: 5100 Pico LE) and field emission scanning electron microscope (Zeiss Sigma model: FEI quanta 250) are used to analyze the surface and morphological behavior of In-Yb_2O_3 films. The existences of elements like Yb,O and In have been determined by energy dispersive X-ray analysis (EDX). The optical property is studied using UV–Vis Spectrometer (JASCO, model: V-770PC). Photoluminescence (PL) spectra are captured at 300 K through Spectrofluorometer (JASCO, model: FP-8300) in the wavelength range 200–750 nm. Finally, the electrical properties of the prepared thin films have been determined using two probe instruments at various temperatures $(30 - 150\ ^{\circ}C)$. Keithley electro-meter (Model: 6517B) is used to study the current Vs voltage (I–V) characteristics of the fabricated Al/ In-Yb_2O_3/p-Si diode. The photo diode property of the diode is analyzed by portable solar stimulator (PEC-L01) at 100 W/m^2 intensity.

Results and discussion

Thickness of In-Yb2O3 films

The thickness of Yb_2O_3 and In-Yb_2O_3 films with indium (In) concentration is revealed in Fig. 2. The thicknesses of the films are found to gradually rise with increasing of indium (In) concentration. The measured film thickness is 156, 282, 394, 548 and 681 nm for 0, 1.5, 2.5, 3.5 and 4.5 wt. % of In-Yb_2O_3 thin films. This is because, the thickness increasing upon the doping levels is likely to come from the fabrication process of thin films. The deposition of films is controlled by film thickness, uniformity and surface morphology. The higher film thicknesses have been observed in 4.5 wt. % of indium (In) concentration. Also, indium (In) concentration may lead to enhance the film thickness and lattice parameters. The deposition parameters with substrate temperature, deposition time, mole ratio, and carrier gas pressure,

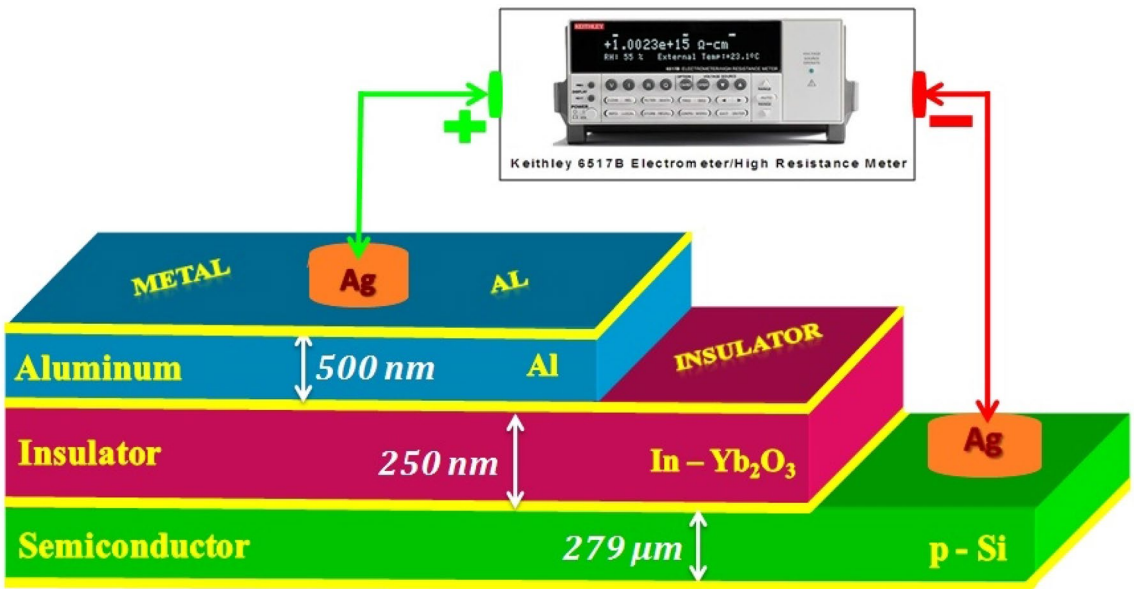


Fig. 1 Schematic diagram of Al/In-Yb_2O_3/p-Si Schottky Barrier Diode

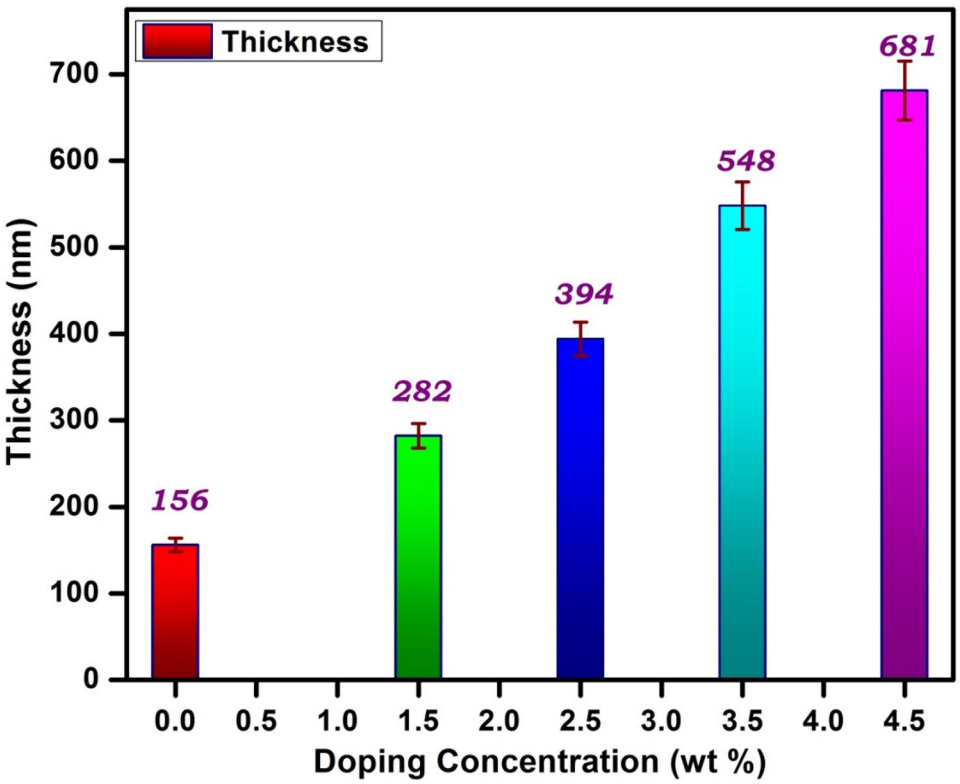


Fig. 2 Thickness variation of the In-Yb_2O_3 thin films for different doping concentrations

determine the growth and quality of the film and hence the JNSP techniques have great influence on developing the thin layer films (Marikkannu et al. 2014).

X-Ray diffraction analysis

XRD analysis of undoped Yb_2O_3 films deposited with different doping concentration like 0.0–4.5 wt. % of indium (In) at 550 °C optimized temperature, are presented in Fig. 3a–e. The XRD patterns of Yb_2O_3 that correspond to the main angle of diffraction peaks are 20.81, 29.52, 34.60, 44.46, 49.37 and 58.56° to their linked (h,k,l) planes of (211), (222), (400), (134), (440) and (622), respectively. The comparison of observed X-ray diffraction patterns with the JCPDS data (65-5792) confirms that the films are indicating the phase pure cubic crystal structure of In-Yb_2O_3 thin films (Mohanraj et al. 2018). The sharp peak present in thus XRD patterns shows good crystalline structure. A (222) predominant peak is the strongest one along with the other observed peaks which indicate that the prepared 4.5 wt.% of In-Yb_2O_3 films has superior potential properties of growth oriented along the (222) crystalline plane. Furthermore, the intensity of (222) peak gradually decreases, which clearly shows that the crystalline size is little falling down with rise in doping concentration to host lattice. However, the minute peaks are disappearing due to increase in the doping concentration (Ben Farhat et al. 2010). Interestingly, no other impurity peaks are found in the XRD patterns, which is clearly indicating the successfully incorporation of In^{3+} ions compared to Yb^{3+} ions which leads to decrease in crystalline size in In-Yb_2O_3 thin films (Lei et al. 2012). The average crystalline size (D) of undoped Yb_2O_3 films and indium (In) doped Yb_2O_3 films is find out using Scherrer equation given below (Balasubramani et al. 2020).

$$Crystalline\ Size\ (D) = \frac{K\lambda}{\beta \cos\theta} \quad (1)$$

where D is the crystalline size, λ is the wavelength of the incident X-ray beam used for measurements and β is the full width half maximum. The average crystalline size of undoped Yb_2O_3 is 11.95 nm. Similarly, the average crystalline size of In doped Yb_2O_3 thin films linearly decreases in the range 9.08–3.95 nm for 1.5–4.5 wt. % doping concentration level and values are presented in Table 1. The minimum crystalline size is observed in higher dopant as the intensity of peaks reduce, indicating increase in full width at half maximum (FWHM). The minimum crystalline size (3.95 nm) with wider FWHM (0.037°) at 4.5 wt.% of In and maximum crystalline size (9.08 nm) with narrow FWHM (0.0189°) at 1.5 wt.% of In are attributed to lattice distortion and increase in nucleation sites with In

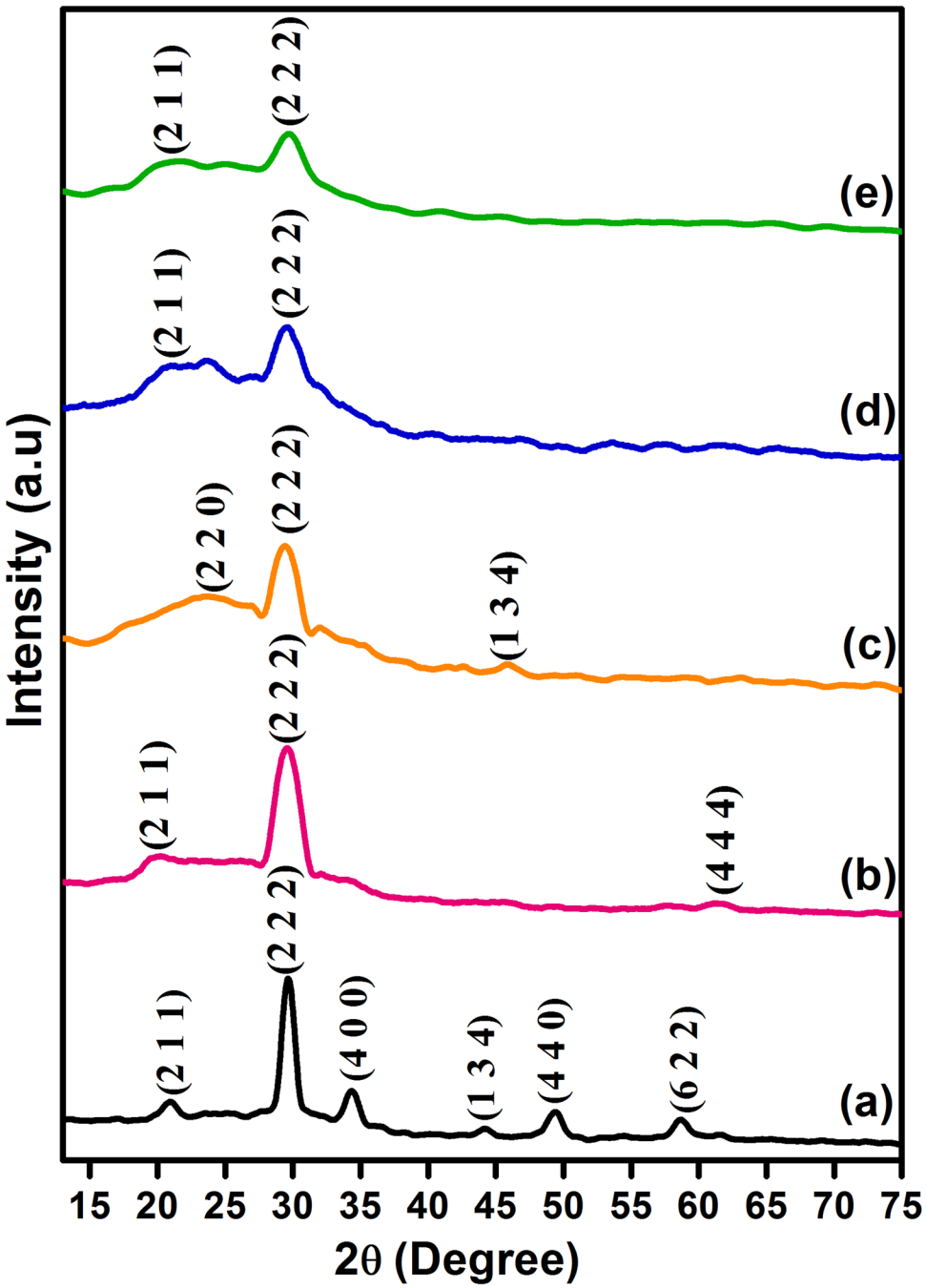


Fig.3 XRD pattern of the In-Yb_2O_3 thin films for different dopant of **a** 0 wt %, **b** 1.5 wt %, **c** 2.5 wt % **d** 3.5 wt % and **e** 4.5 wt %

Table 1 Structural parameters of the prepared undoped and indium (In) doped Yb_2O_3 thin films

In content (wt %)	Thickness (nm)	FWHM (in Rad)	D (nm)	$\varepsilon \times 10^{-3}$ (lines^{-2} m^{-4})	$\delta \times 10^{16}$ lines cm^{-4}	SF$\times 10^{-2}$
0	156	0.0145	11.300	3.320	0.991	1.150
1.5	282	0.0189	9.080	4.760	2.203	1.270
2.5	394	0.0242	7.120	5.980	3.870	1.520
3.5	548	0.0321	5.130	7.690	5.632	1.880
4.5	681	0.0370	3.950	8.900	6.760	1.910

doping or due to the saturation of In over Yb_2O_3 lattice as shown in Fig. 4 (Zargouni et al. 2020b). Also, the dislocation density (δ), micro strain (ε), & stacking fault (SF) are obtained by Eqs. (2–4) (Balasubramani et al. 2020) and registered in Table 1.

$$\text{Dislocation density}\,(\delta) = \frac{1}{D^2} \tag{2}$$

$$\text{Micro strain}\,(\varepsilon) = \left[\left(\frac{\lambda}{D\sin\theta}\right) - \left(\frac{\beta}{\tan\theta}\right)\right] \tag{3}$$

$$\text{Stacking fault}\,(SF) = \left[\left(\frac{2\pi^2}{45(3\tan\theta)^{\frac{1}{2}}}\right) \times \beta\right] \tag{4}$$

Figure 4 reveals that the δ, ε, and SF are increased as result of dopant gets increased. These results clearly observe that the key reason of falling with crystalline size is linked with decrease in dislocation density, micro strain, and stacking fault due to the large number of grain boundaries, disorder in crystal with defects, interstitials/void that confine the nucleation/growth of new nuclei and so the size is reduced. From these results, we notice that increases in doping concentration sturdily affect the structural constraints.

Surface morphology analysis

FESEM images are exposed in Fig. 5a–e for undoped Yb_2O_3 and In doped Yb_2O_3 thin films with different doping concentration of 0, 1.5, 2.5, 3.5 and 4.5 wt. % at an optimized substrate temperature 550 °C. The film surface morphology exhibits continuous variation on doping level into Yb_2O_3 film surface. The indium doping concentration has highly dominion in the surface morphology of In-Yb_2O_3 thin films. Figure 5a shows that randomly oriented, crack free and smooth surface of the fine tiny globular-like structure having an average size of the particle 11 nm, are found to the undoped Yb_2O_3 thin films. Figure 5b, c reveals that the films non-uniform jems stone-like homogeneous cubic particles with irregular voids are observed (Raj Mohamed et al. 2016). This result indicates the reduced particles have a high surface to volume ratio. Therefore, the size of particle in In-Yb_2O_3 films is lessened by increase in doping concentration (1.5–2.5 wt %) into Yb_2O_3 lattice sites. Furthermore, a small reduction in the grain size is observed with increases in the indium (In) doping concentration as shown in Fig. 5d, e. Interestingly, the surface morphology does not change the structure and only dense of the particle is slightly decreased with increasing dopant (Petroff et al. 1973). These results show that particle size is reduced in higher dopant because the dopant creates the defect in Yb_2O_3 lattice (Katsuno et al. 2011). Moreover, the surface morphology confirms to reduce the leakage current of the device and improve the electrical conductivity. Therefore, the reduced particle sizes are evidenced by the XRD parameters. Hence, the incorporation of indium (In) concentration highly affects the surface morphology of the In-Yb_2O_3 films.

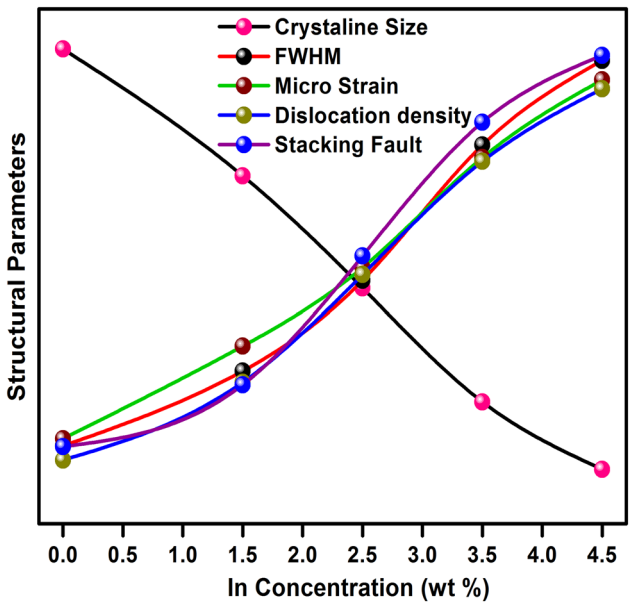


Fig. 4 Structural parameters Vs indium (In) content of different wt%

Topographic analysis

Figure 6a–c demonstrates the 2d, 3d topographic images of AFM along with their surface roughness histogram of In-Yb_2O_3 thin films deposited at optimized temperature 550 °C for 4.5 wt % dopant. Figure 6a exposed non-uniform distribution and very fine smooth surface are observed from 2d topography. Figure 6b clearly shows that the small particles get together to build conical pyramid like assembly with some voids identified by 3d topography. Figure 6c shows that surface roughness histogram measures average surface roughness R_a (7.215 nm) and area root mean square (RMS) (10.34 nm) with the addition of indium (In) concentration. From these results, which might be due to reduce crystalline size, altered nucleation, boundaries and merging of grains are decreased. Furthermore, when doping concentration increases, it is confirmed by transparency that there is growing in the thickness of thin film. This is possible due to the increase in the occurrence of In ions on the host Yb_2O_3 film surface. The surface morphology of Yb_2O_3 films can be modified by adding In dopant, which might significantly affect the properties. Thus, the morphological variations are good agreements with FESEM image and XRD parameter

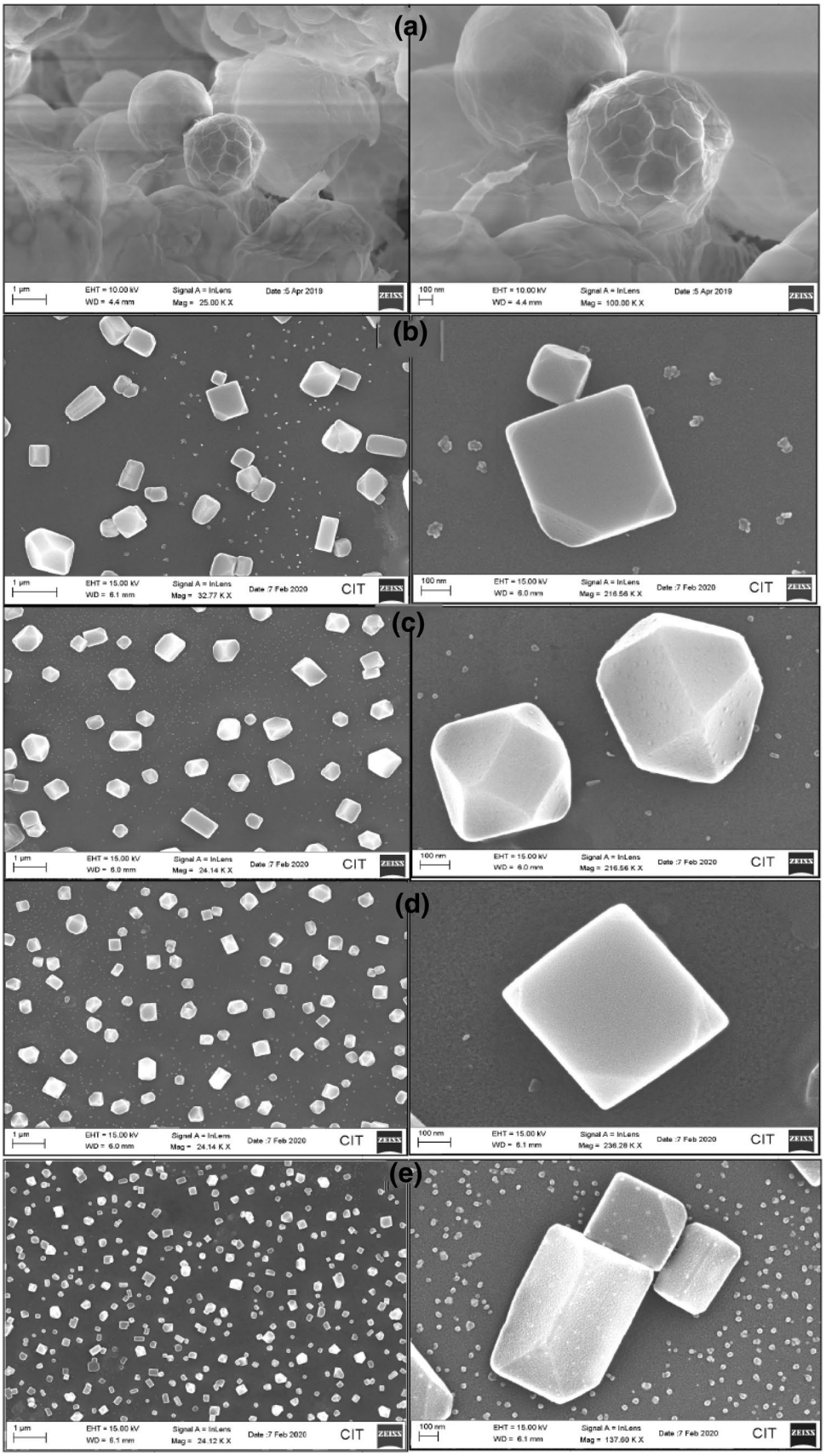


Fig. 5 FESEM images of the In-Yb_2O_3 films with different dopant **a** 0 wt% **b** 1.5 wt% **c** 2.5 wt% **d** 3.5 wt % **e** 4.5 wt %

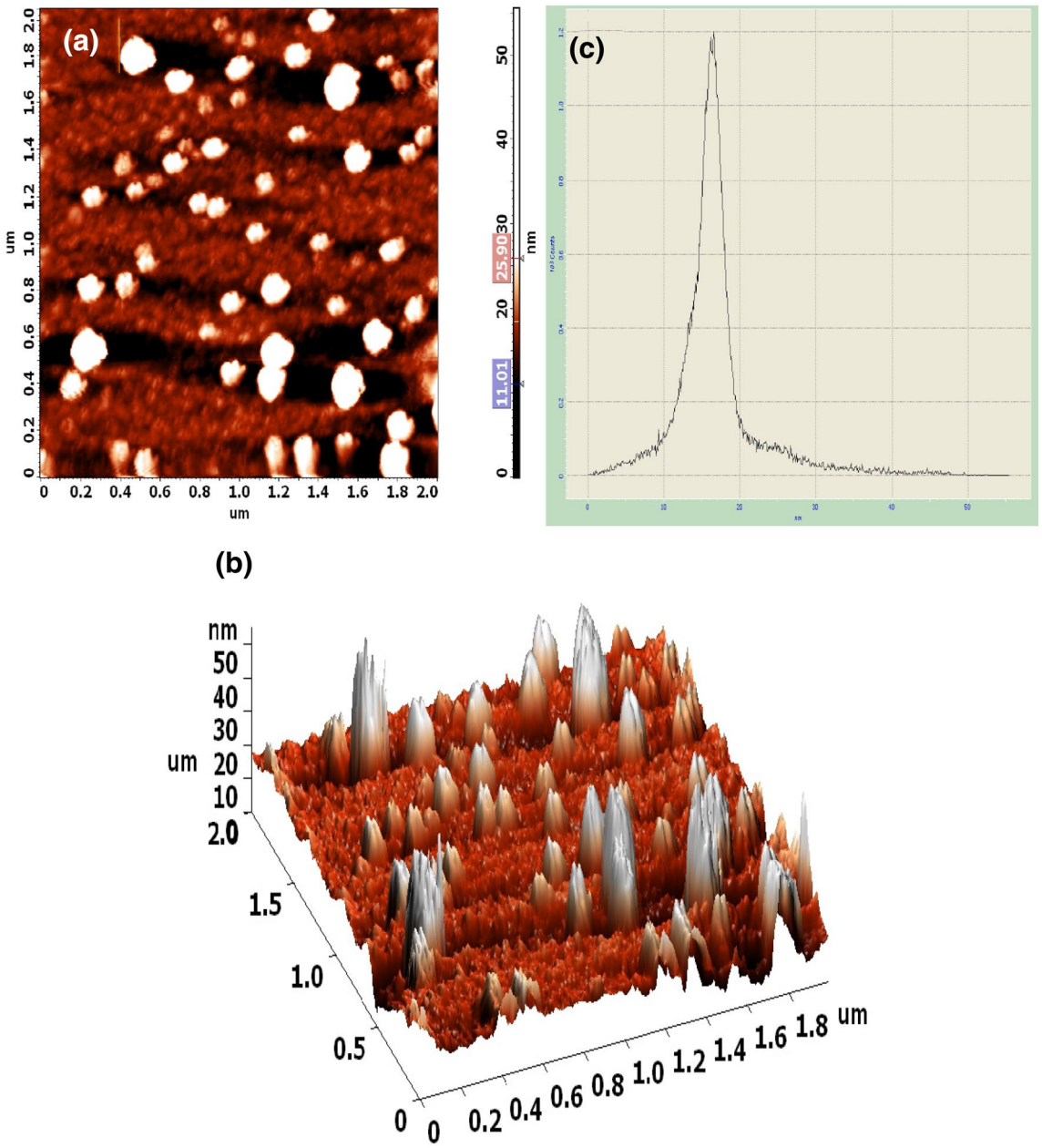


Fig. 6 Topographic (AFM) Images of 4.5 wt % In doped Yb_2O_3 film **a** 2d image **b** 3d image **c** Histogram

favors to advance the conductivity of films, which is suitable for SBDs (Sarath babu et al. 2020).

Elemental composition analysis

Figure 7a–e shows the EDX spectra of the undoped Yb_2O_3 films and doped Yb_2O_3 films deposited at different doping concentration such as 1.5–4.5 wt % with substrate temperature 550 °C. It is clearly indicating the Yb, In, and O peaks are close to stoichiometry ratio in In-Yb_2O_3 thin films. The atomic % of Indium concentration increases from 1.81, 3.13, 4.43, and 7.23 In-Yb_2O_3 films coated with different doping concentration. Particularly, ytterbium concentration is little falling with rise in oxygen content due to the increase in doping concentration. There are no peaks observed related to elements other than indium (In), ytterbium (Yb), and oxygen (O) in the EDX spectra. From the EDX results, the In-Yb_2O_3 thin films which indicate the strong influence to In with Yb at higher doping concentration. These results clearly mention that the indium (In) plays an important role in better optical behavior of the In-Yb_2O_3 films and enhances the device performance (Raja et al. 2019).

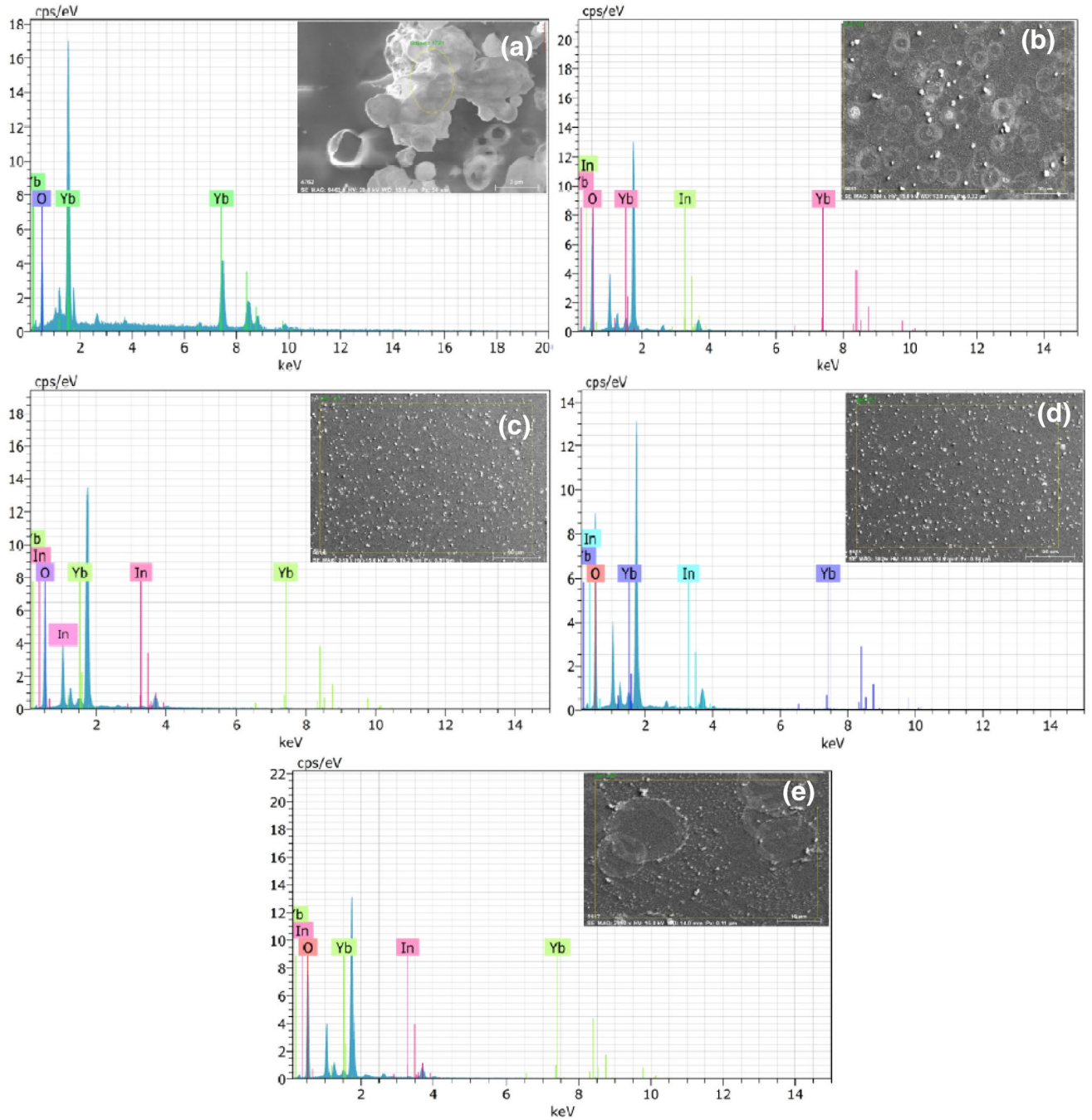


Fig. 7 Elemental analysis of the In-Yb_2O_3 films with different doping concentrations. **a** 0 wt% **b** 1.5 wt% **c** 2.5 wt% **d** 3.5 wt % **e** 4.5 wt %

Photoluminescence analysis

The intrinsic optical characteristics of the samples are further elucidated by photoluminescence (PL) spectroscopy. Figure 8a, b indicates the room temperature PL spectra of undoped Yb_2O_3 and different doping concentration such as 1.5–4.5 wt % of In-Yb_2O_3 thin films deposited an optimized substrate temperature 550 °C. The undoped Yb_2O_3 films indicate a PL peak in the board UV emission peak around 299 nm as shown in Fig. 8a. Figure 8b indicates that, when the dopant increases, the film exhibits strong emission sharp ultraviolet (UV-NBE) peak around 361 nm and additional blue emission peak around 491 nm and also sharp visible green emission peak 521 nm which clearly shows that the peak position is slightly shifted to higher energy side when the dopant increases. Also, the PL emission peak intensity is varying with increase in doping concentration such variation in emission intensity might be attributed to defects created

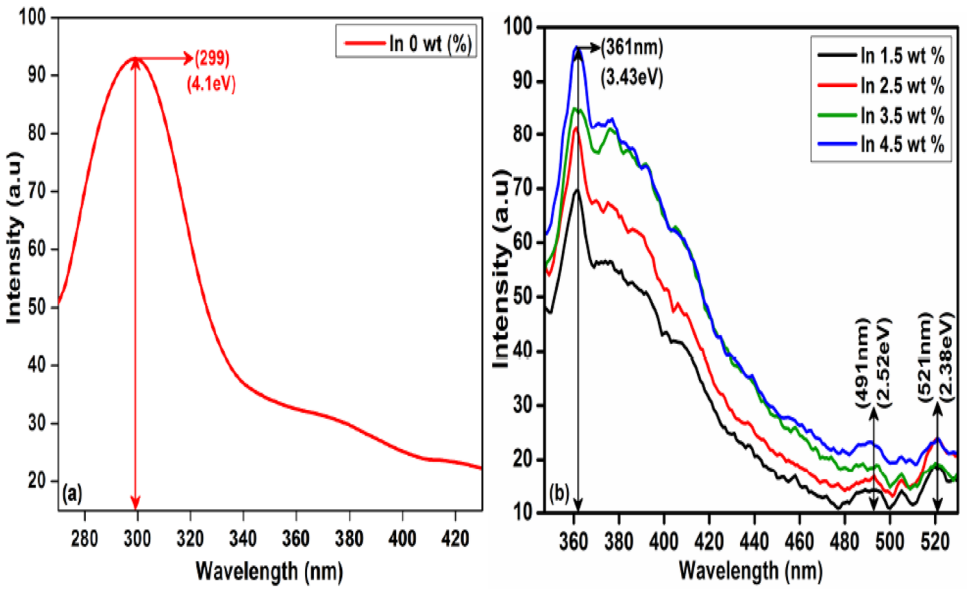


Fig. 8 Photoluminescence spectrum of **a** undoped Yb_2O_3film **b** In doped Yb_2O_3 films

from distortedness in the films when doped with In. Furthermore, the blue and green emission bands owing to the presence of interstitial oxygen vacancies and intrinsic defects due to doping concentration. These results are enhancing the optional behavior and they help to improve device performance which is preferable for SBDs, the highest PL emission intensity was observed for 4.5 wt % In-Yb_2O_3 films compared with other deposited films (Bhuvaneswari et al. 2020). Hence, these results correlated with the surface morphology and structural changes with the increases in doping content which is observed in SEM and XRD results.

Optical absorbance analysis

Figure 9a–d represents the variation optical parameters of indium (In) doped ytterbium oxide thin films with optimized substrate temperature 550 °C. Figure 9a visualizes that undoped Yb_2O_3 indicates lower absorption (A) compared with doped thin films. It may be due to higher transmittances (T) of the film. In addition, In-Yb_2O_3 films source a sharp absorption edge increases gradually in the UV region is exhibited with the range from 225 to 330 nm, ic < 350 nm, which increases with higher In wt %. This behavior is owing to the deep bluish coloration of the film with grain boundaries and enhancement of carrier concentration due to the addition In ions in the Yb_2O_3 lattice. The maximum absorbance is observed for higher doping content of 4.5 wt % in In-Yb_2O_3 thin films. Figure 9b indicates that transmittance spectrum of undoped Yb_2O_3 thin films show a very low transmittance than doped Yb_2O_3 thin films. The transmittance spectra of In-Yb_2O_3 indicates rise in transmittance till NIR region. It further rises to 70% in VIS area and becomes stable in NIR region. The T value increases with increase in doping concentration 3.5 wt % and slightly decreases when the doping concentration is increased to 4.5 wt %. It might be attributed to rise in photons, due to the increase in scattering through defects generated by dopant (Desai 2018). Another reason is increases in film thickness and free carrier photon absorption promote in lessening of T with higher doping content. From the UV–Vis spectra, the optical energy gap (eV) values are obtained from the following relation (5) (Vivek et al. 2019b)

$$\text{Band gap}\,(\alpha h\nu) = A(h\nu - E_g)^n \tag{5}$$

Here α stands for co-efficient to absorption, hν is energy, A is constant, E_g is energy band gap values determined from Tauc's plot, among $(\alpha h\nu)^{1/2}$ vs $(h\nu)$ for In-Yb_2O_3 thin films as shown in Fig. 9c. When n is ½ specified, indirectly permitted transitions and intercept on E-axis give the E values. The energy gap values are 3.58, 3.62, 3.66, 3.70 and 3.75 eV, respectively, for undoped Yb_2O_3 and In-Yb_2O_3 films are noticed from extrapolating of vertical strait line to E-axis. The calculated optical energy gap is found to be increased when there is a rise in In concentration (Muralidharan et al. 2018). The variation of energy gap due to the formation of the film layer and the donor atoms (In) may provide additional carrier causing the shifting of fermi level toward conduction band. Furthermore, the energy gap could also be affected by changing the particle size with dopant as in the nano meter range. In concentration provides the shift of the energy gap toward higher energy, which is appropriate for MIS structures SBDs. The absorption co-efficient (α),

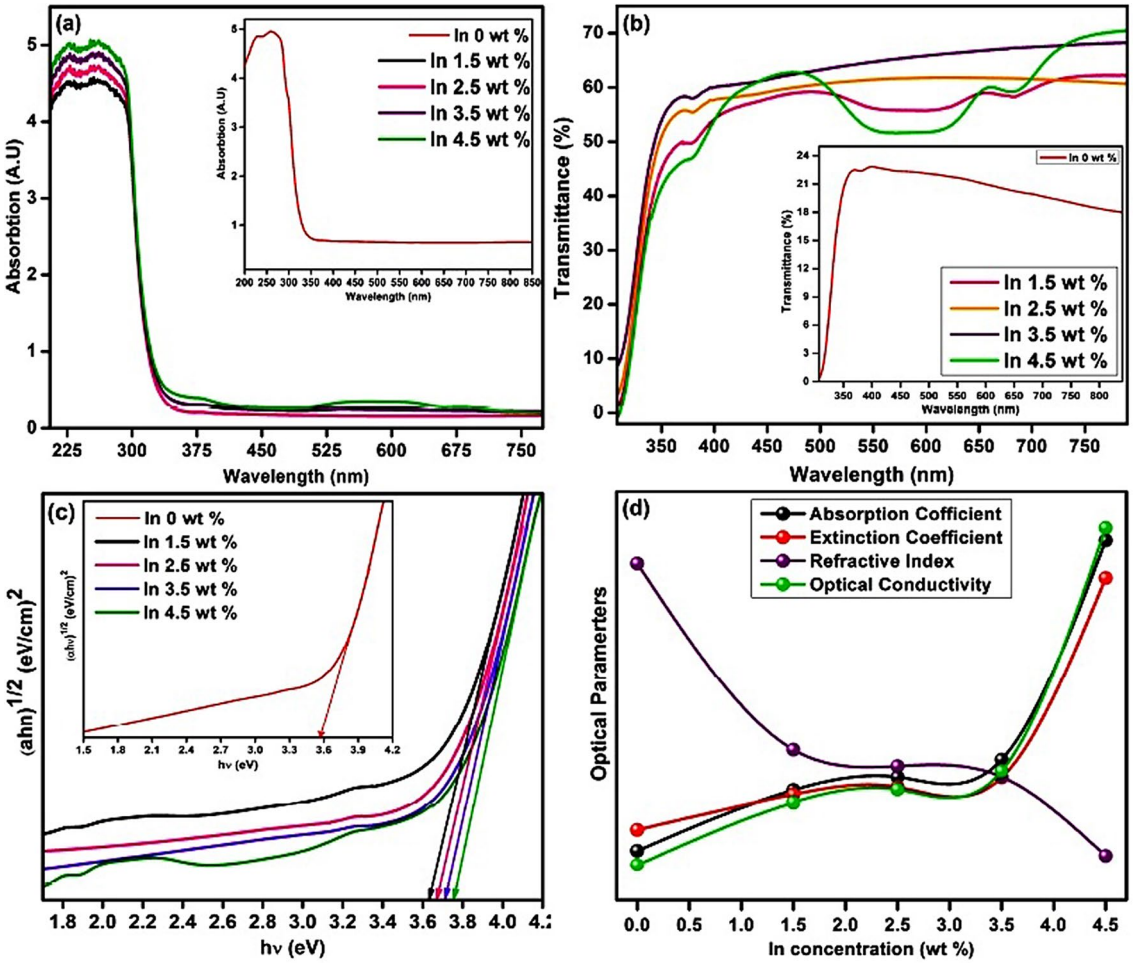


Fig. 9 **a** Absorbance Spectra, **b** Transmittance spectra, **c** plots of $(\alpha h\nu)^{1/2}$ Vs $h\nu$, and **d** Average optical parameters for undoped Yb_2O_3 film and indium (In) doped Yb_2O_3 thin films obtained at different doping content

refractive index (n), extinction co-efficient (k) and optical conductivity (σ_{opt}) are assessed by the following Eqs. (6–9) (Vivek et al. 2019b).

$$\text{Absorption co}-\text{efficient}\,(\alpha) = \left[\frac{1}{t}\right]\ln\left[\frac{1}{T}\right] \tag{6}$$

$$\text{Refractive index}\,(n) = \left[\frac{1+R}{1-R}\right] + \left[\sqrt{\frac{4R}{(1-R)^2 - k^2}}\right] \tag{7}$$

$$\text{Extinction co}-\text{efficient}\,(k) = \left[\frac{\alpha\lambda}{4\pi}\right] \tag{8}$$

$$\text{Optical conductivity}\,(\sigma_{opt}) = \left[\frac{nc\alpha}{4\pi}\right] \tag{9}$$

The variation of α, k, n and σ_{opt} values with different doping concentration as shown in Fig. 9d.

The refractive index (n) of the film steeply reduces between 2.79 and 2.296. The minimum refractive index value 2.296 observed in higher doping concentration of 4.5 wt %, is due to variation of packing density and higher film thickness. The values of α, k, and σ_{opt} parameters of the In-Yb_2O_3 films noticed with maximum values like $\alpha = 6.028 \times 10^{-6}$ (cm^{-1}), $k = 0.1935$ and $\sigma_{\text{opt}} = 4.119 \times 10^{14}$ (S/cm) are obtained by 4.5 wt % of In concentration. These results are used for influencing the electronic transition among two bands ic. (Valance band and Conduction band). From the optical studies, we find that incorporation of In sturdily affects the optical constraints of the In-Yb_2O_3 films, which can have an impact of the Schottky barrier diodes (Shkir et al. 2020).

D.C electrical analysis

The temperature dependence of DC electrical conductivity (σ_{dc}) of undoped Yb_2O_3 and In-Yb_2O_3 thin films for different indium (In) content like 1.5–4.5 wt % are measured by two probe step-up with the variation temperature from 30 to 150 °C in an increases of 20 °C along with constant potential voltage from 10 to 100 V in an increase of 10 V. The obtained resistivity (ρ) values of all the films are specified in Table 2 and noticed that the undoped Yb_2O_3 thin films owning a ρ value of ~ 1.11×10^{15} Ω cm, which is found to reduce linearly to ~ 3.88×10^{13} Ω cm, while there is increase in dopant (Marnadu et al. 2018). This will be helpful in getting the better charge carrier mobility in it. The σ_{dc} is determined by following Eq. 10 (Vivek et al. 2019b).

$$\text{Electrical conductivity}\ (\sigma_{dc}) = \frac{t}{RA} s/cm \tag{10}$$

Here R, t and A are related to resistance, thickness, and area of the film. I-V parameters are investigated and exposed in Fig. 10a–e. Figure 10 indicating that voltage is proportional in nature to current at all measured temperatures (30–150 °C). The conductivity of In-Yb_2O_3 thin film is increased by rise in dopant. The maximum electrical conductivity (σ_{dc}) is obtained for higher doping concentration with 4.5 wt %. The average electrical conductivity varied from 1.08×10^{-15} – 2.88×10^{-14} S/cm. The maximum average conductivity is obtained for rising indium (In) content, which is attributing to oxygen vacancies and create extra free electrons in valence band (Caglar et al. 2009). Furthermore, the dopant supplies additional charge carriers (electrons + holes) in the host ions. In addition, the addition of indium (In) ions increases the volumetric rate needed for ionic haulers to drift in Yb_2O_3 films. However, this will advance mobility of ions in the film to attain improved σ_{dc}. The obtained σ_{dc} (10^{-15}—10^{-14} S/cm) indicating an insulating behavior is supported to schottky barrier diodes (Dogru Balbasi et al. 2020). In these results, the films help as an insulating layer in Al/In-Yb_2O_3/p-Si SBDs to improve their performance. The activation energy E_a is determined from Arrhenius plot using the following Eq. 11 (Vivek et al. 2019b).

$$\text{Activation Energy}\ (\sigma_{dc}) = \sigma_o \exp\left[\frac{-E_a}{K_B T}\right] \tag{11}$$

Here σ_0, E_a & K_B stand for constant, activation energy, Boltzmann constant and T is absolute temperature. Figure 11 shows the Arrhenius diagram of (1/T) (K^{-1}) vs ln (σ) for In-Yb_2O_3 thin films and it is observable from the plot that the indium (In) (σ) values increase gradually with (1/T) (K^{-1}). The E_a is a key parameter to determine the electrical characteristics of In-Yb_2O_3 thin films. The calculated average E_a shrinks from 0.395 to 0.284 eV with increase in doping concentration. These results indicate that indium ions successfully incorporate to the Yb_2O_3 ions. Furthermore, the changes in activation energy are due to surface structure and imperfections of higher doping concentration of films (Dogru Balbasi et al. 2020). The obtained mean conductivity is improved whereas the linked mean resistivity and E_a are lessened. Figure 12 clearly shows average electrical conductivity and average activation energy Vs In content. From the conductivity results, we attain extremely suitable films as layer at interface in MIS to enhance the actions of device.

Table 2 Electrical parameters of undoped and indium (In) doped Yb_2O_3 thin films

InContent (wt %)	Resistivity (ρ) (Ω.cm)	Average conductivity (σ_{dc}) (S/cm)	Activation energy (E_a) (eV)
0	1.11×10^{15}	1.08×10^{-15}	0.395
1.5	2.42×10^{14}	4.60×10^{-15}	0.323
2.5	1.54×10^{14}	7.11×10^{-15}	0.301
3.5	9.21×10^{13}	1.19×10^{-14}	0.292
4.5	3.88×10^{13}	2.88×10^{-14}	0.284

I-V nature of Al/In-Yb2O3/p-Si SBD

Fig. 13a–e visualizes I-V nature of fabricated MIS diode. Ohmic behavior of MIS diode is analyzed for different doping concentration such as 1.5, 2.5, 3.5 and 4.5 wt % of indium (In) concentration. The parameters of MIS diodes are inspected in dark and illumination surroundings using I-V. Figure 14 reveals both reverse and forward current of Schottky barrier diodes measured by applying bias voltage -3 to + 3 V (in stet of 0.3 V) of potential. The current density ($J = I/A$) of Schottky barrier diode for $V \geq 3K_BT/q$ is determined by thermionic emission theory and given by following Eq. 12 and 13 (Marnadu et al. 2019)

$$\text{Current density}\ (I) = I_o \exp\left[\left(\frac{qV}{nK_BT}\right) - 1\right] \tag{12}$$

$$\text{Reverse saturation current} I_o = AA^*T^2 \exp\left(-\frac{q\Phi_B}{K_BT}\right) \tag{13}$$

Here I_o is reverse saturation current, q is charge, V is voltage, n is ideality factor, Φ_B is effective barrier height and K_B is Boltzmann constant, T is the temperature, A is the area of the diode and A* effective Richardson constant (32 A/cm^2.K^2 for p-Si). Besides, the I_0 values can be derived from intercept of linear area of ln(I)—V curve in forward

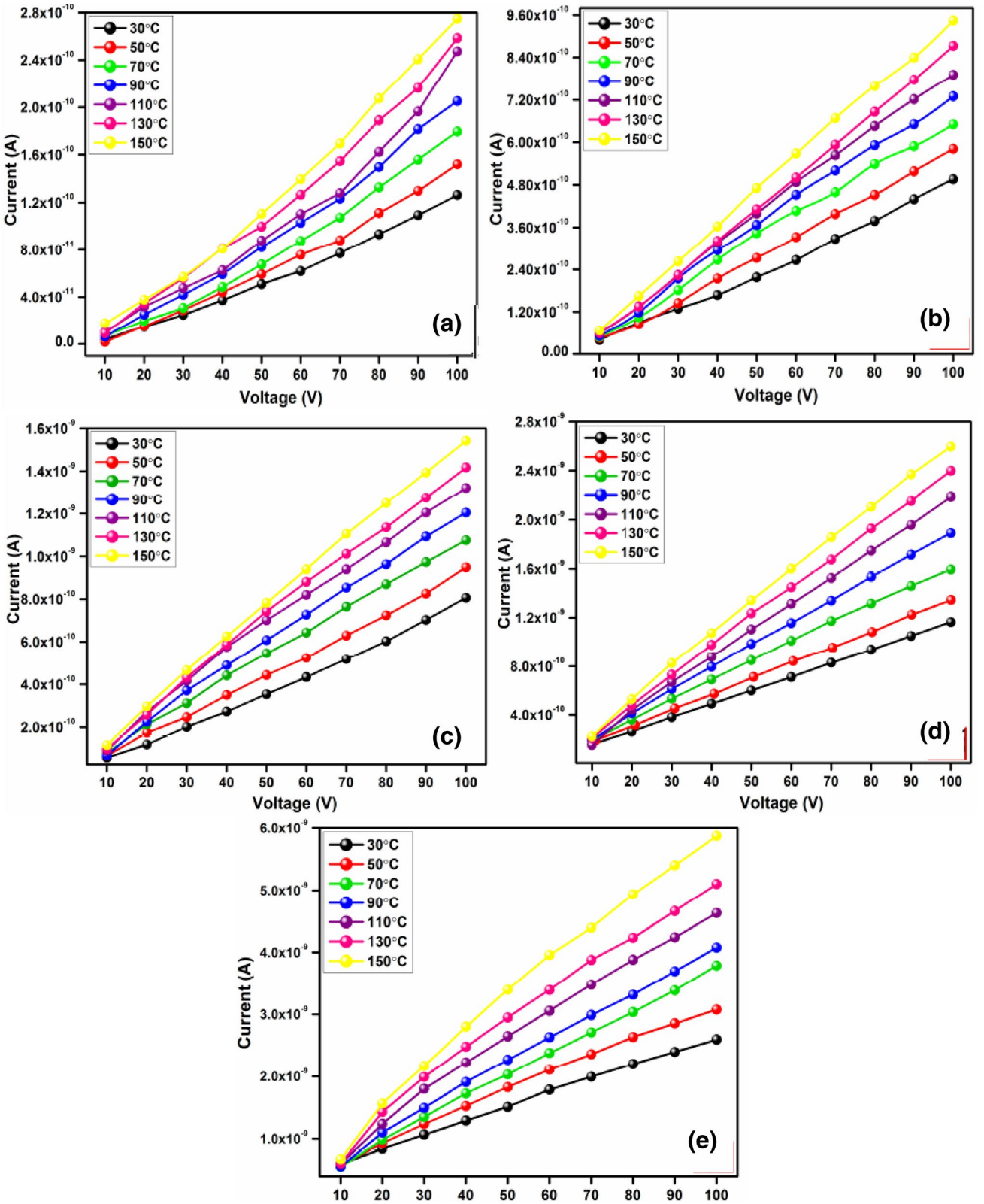


Fig. 10 Current –Voltage (I-V) plots of the prepared films at different temperature. **a** undoped Yb_2O_3 and **b**–**e** 1.5, 2.5, 3.5, and 4.5 wt % of indium (In) doped Yb_2O_3 thin films

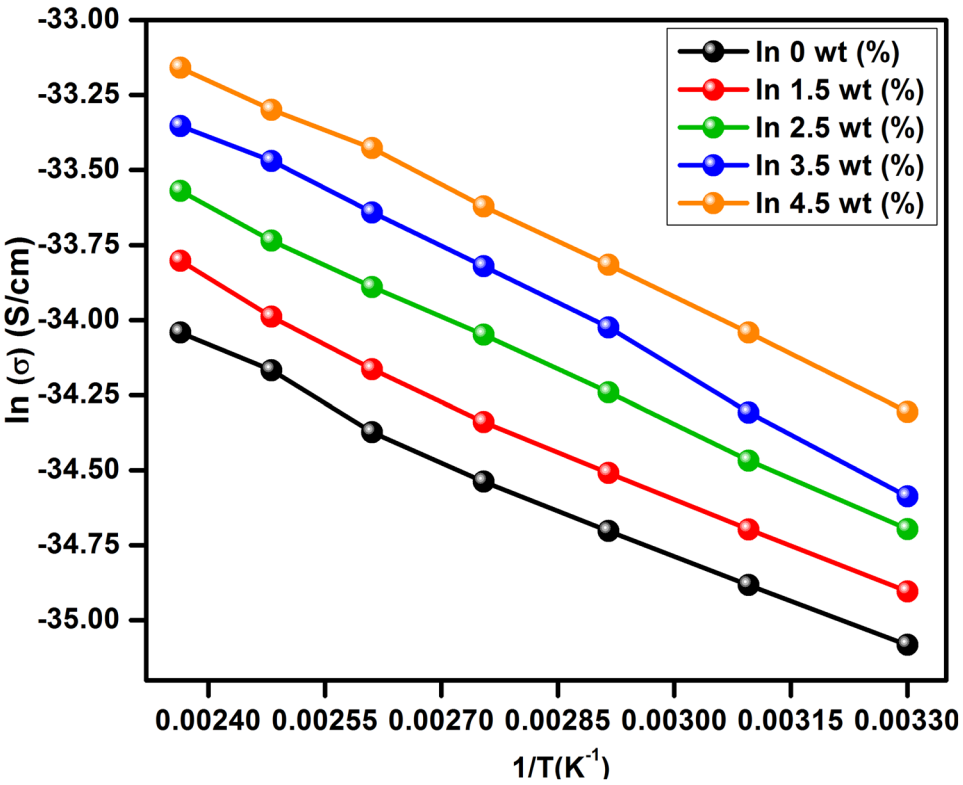


Fig.11 Arrhenius plots of ln (σ) vs 1/T of In-Yb_2O_3 films for different indium (In) wt%

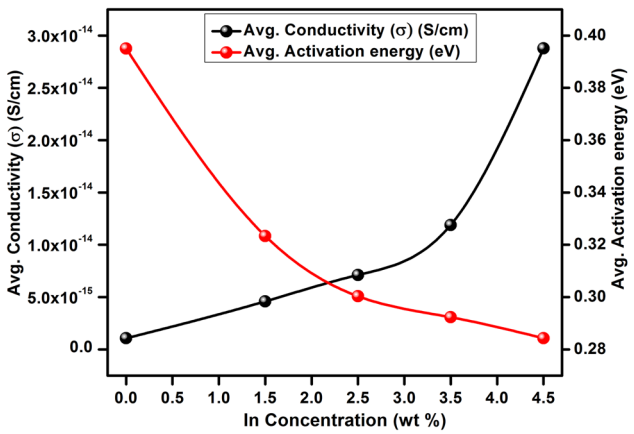


Fig. 12 Average electrical conductivity and Average activation energy versus indium (In) concentrations (wt %)

bias. As shown in I-V curves in Fig. 13a–e, each MIS diodes indicate positive response on testing of device under illumination. The outcomes suggest photoconducting behavior of developed diodes. The attained I_o values are noticed between 1.05×10^{-6}–7.39×10^{-5} A in dark, however, improved and found between 1.74×10^{-5}–4.19×10^{-4} A in case of illumination, all the values are summarized in Table 3 (Kahraman et al. 2020; Janardhanam et al. 2020). The obtained results suggest that, the device performance and good (σ) values of the Al/In-Yb_2O_3/p-Si diodes have improved due to the successfully incorporation of dopant (Lapa et al. 2020). In addition, the n and Φ_B values are determined by the following Eqs. 14 and 15 (Marnadu et al. 2019).

$$\text{Ideality factor}\,(n) = \left[\frac{q}{K_BT}\left(\frac{dV}{d(InJ)}\right)\right] \tag{14}$$

$$\text{Barrier height}\,\left(\Phi_B\right) = \left[\frac{K_BT}{q}In\left(\frac{AA^*T^2}{I_o}\right)\right] \tag{15}$$

Fig. 14a–e clearly indicates ln(J)-V plots of Al/In-Yb2O3/p-Si with different indium (In) concentration. Ideality factor (n) values are derived through slope of linear region of ln (J)-V curve. The obtained n and Φ_B quantities are presented in Table 3. It is clear that for the increase in indium (In) concentration, the values of n is reduced from 2.331 to 2.152 in dark state. Fascinatingly, the MIS diodes studied below illumination condition denoting the lesser n values 2.07–1.79 are compared to dark condition. As n values are > 1, the Al/In-Yb_2O_3/p-Si SBDs exhibited non-ideal nature in forward bias I-V at appropriately greater voltage, signify a transport nature than emission of thermionic (Balaji et al. 2020). This may be attributed to the generation of (e^-—h^+) pair of recombining in region of depletion, current nature owed to sub states in surface/current diffusion as secondary issues (Uma et al. 2019). The greater n values might be linked to existence of a native oxide thin layer at interfacial, a broad spreading of barrier inhomogeneities,

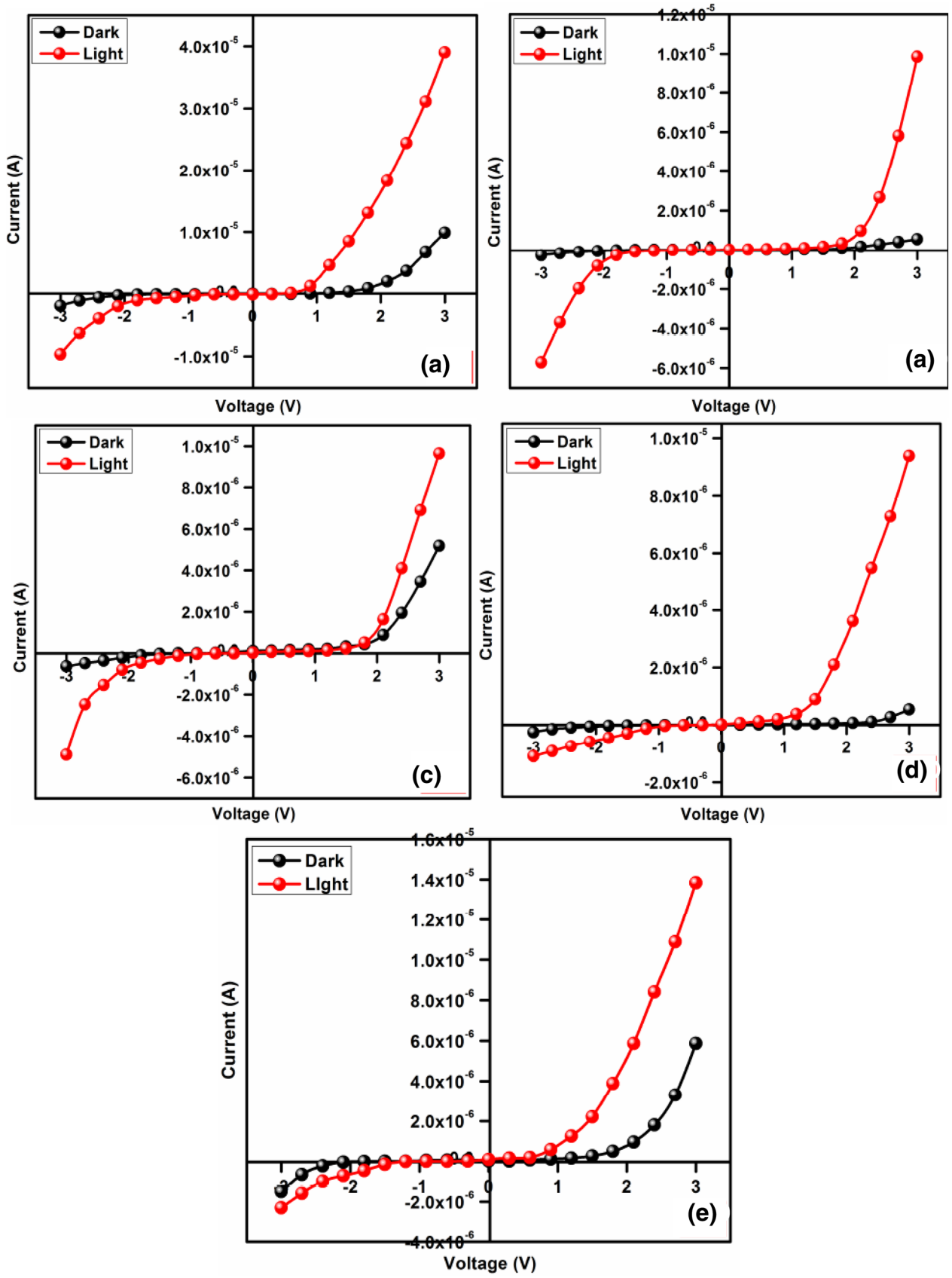


Fig. 13 I-V plots of Al/In-Yb_2O_3/p-Si Schottky barrier diodes with different doping concentrations **a** 0 wt% **b** 1.5 wt% **c** 2.5 wt% **d** 3.5 wt % **e** 4.5 wt %

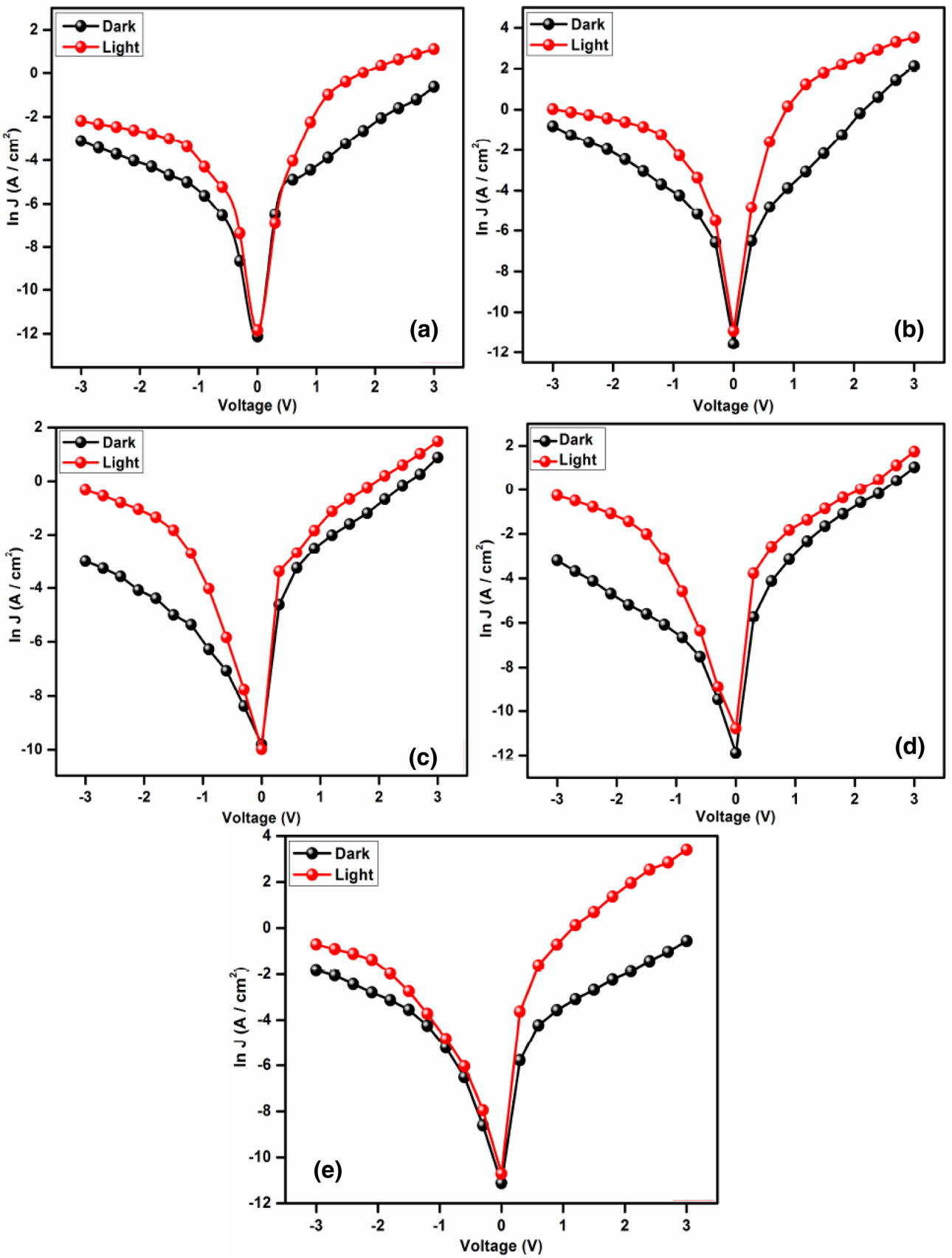


Fig. 14 ln J-Vplots of Al/In-Yb_2O_3/p-Si Schottky barrier diodes with different doping concentrations **a** 0 wt% **b** 1.5 wt% **c** 2.5 wt% **d** 3.5 wt % **e** 4.5 wt %

Table 3 Electrical parameters of Al/In-Yb_2O_3/p-Si Schottky Diodes with different indium (In) dopant

InContent (wt.%)	Ideality factor (n)		Barrier height Φ_B (eV)		Saturation current (I_o) (A)		Photo sensitivity
	Dark	Light	Dark	Light	Dark	Light	P_s (%)
0	2.331	2.075	0.702	0.606	1.05×10^{-6}	1.74×10^{-5}	233.48
1.5	2.272	2.011	0.723	0.615	3.94×10^{-6}	4.85×10^{-5}	827.58
2.5	2.215	1.967	0.753	0.639	2.06×10^{-5}	1.83×10^{-4}	1073.43
3.5	2.184	1.871	0.778	0.679	3.28×10^{-5}	2.61×10^{-4}	2006.92
4.5	2.152	1.791	0.803	0.692	7.39×10^{-5}	4.19×10^{-4}	3845.58

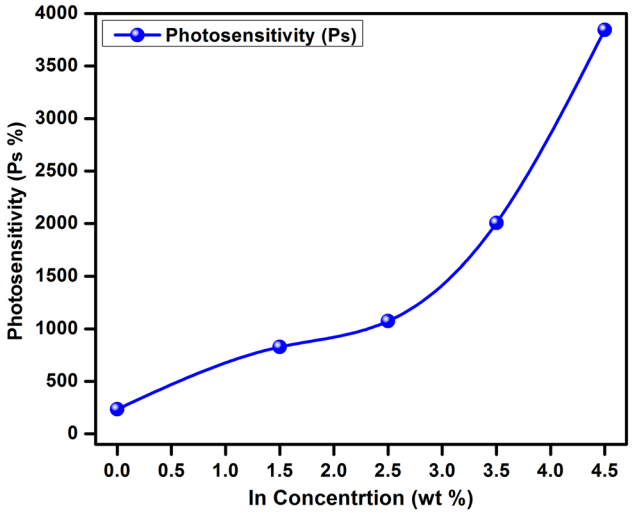


Fig. 15 Photosensitivity of Al/In-Yb_2O_3/p-Si SBDs with different indium (In) dopant

and to bias Φ_B dependence (Di Bartolomeo et al. 2017). Another cause comprises a specific interface state spreading, drop of potential at interface layer, effect of image force, and the tunneling current through interface for higher ideality factor values (Rajagopal Reddy et al. 2015; Tataroglu and Altindal 2008). Furthermore, the increase in contents of carriers and lessening in dependent resistance at larger dopant leads to increase in Φ_B and reduced n values. Inclusively, the barrier height (Φ_B) was found to increases gradually under dark and illumination condition with higher dopant of In-Yb_2O_3 thin films. The observed values of barrier height Φ_B in dark condition 0.702–0.803 eV and illumination condition 0.606–0.692 eV are mentioned in Table 3. Additionally, the percentage of photosensitivity (Ps) of the Al/In-Yb_2O_3/p-Si SBDs can be written as Eq. 16 (Marnadu et al. 2019)

$$\text{Photosensitivity } P_s(\%) = \frac{I_{Ph} - I_D}{I_D} \times 100 \tag{16}$$

Here I_{Ph} and I_D are photo and dark currents of Schottky diode. The calculated values of P_s are varied between 233.48 and 3845.58% with indium content (see Fig. 15). These results are principally owed to light wavelength and rate of absorption of layer of interface as shown in Fig. 15 and values are summarized in Table 3. As a result, the higher Φ_B, P_s and minimum n values are obtained for Al/In-Yb_2O_3/p-Si Schottky barrier diode having higher indium (In) doping concentration with 4.5 wt % in both dark and illumination condition.

Conclusion

A magnificent demonstration of enormously sensitive Al/In-Yb_2O_3/p-Si SBDs has been done by employing various In doping concentration. The structures, opto-electrical properties of the interfacial layer (In-Yb_2O_3) are investigated through various techniques. The XRD analysis show the mono-crystalline nature such as cubic structure of In-Yb_2O_3 films and D_{avg} value decreases in higher doping concentration of 4.5 wt %. The jems stone-like structure with non-uniform surface morphology is recorded through FESEM image. The extreme absorption and wide energy gap of (3.75 eV) is noticed for 4.5 wt % of In-Yb_2O_3 films. The elemental composition spectra confirmed the presence of Yb, In, and O. The topographic studies observe reduction in roughness and RMS values on rising the In doping concentration in In-Yb_2O_3 films. The PL spectrum of In-Yb_2O_3 thin films indicates that strong and broad emission bands at 361 nm. I-V characteristic reveal that the 4.5 wt% In-Yb_2O_3 films give a larger conductivity of 2.88×10^{-14} S/cm. All the Al/In-Yb_2O_3/p-Si SBDs are displayed positive photo conducting behavior. Notably, 4.5 wt % of SBDs is shown under dark and illuminated condition with lowest n values of 2.152 and 1.791. From all the above results, we identify the 4.5 wt % of Al/In-Yb_2O_3/p-Si SBDs is perfectly matched for high-speed switching applications.

Acknowledgements The authors would like to express their gratitude to Advance Research Instrumentation Centre (ARIC), Sri Ramakrishna Mission Vidyalaya College of Arts and Science, Coimbatore for providing instrument facilities. Also, the author Mohd Shkir from KKU would like to express his gratitude to Deanship of Scientific Research at King Khalid University, Abha, Saudi Arabia for funding this work through Research Groups Program under Grant No. R.G.P.2/60/42.

Author's contribution K. S. Mohan contributed to writing of the original draft, validation, investigation and methodology. A. Panneerselvam contributed to writing, supervision, review and editing. J. Chandrasekaran contributed to review and editing. R. Marnadu contributed to validation, investigation, methodology, writing of the original draft, review and editing. Mohd. Shkir contributed to writing of the original draft, review and editing.

Declarations

Conflict of interest The authors declare that they have no competing interests.

References

Asubay S (2011) The electrical characteristics of Al/p-InP Schottky contacts. Microelectron Eng 88:109–112. https://doi.org/10.1016/j.mee.2010.09.00

Balaji M, Chandrasekaran J, Raja M (2016) Role of substrate temperatureon MoO_3 thin films by the JNS pyrolysis techniquefor P-N junction diode application. Mater Sci Semicond Process 43:104–113. https://doi.org/10.1016/j.mssp.2015.12.009

Balaji M, Chandrasekaran J, Raja M, Marnadu R, Ramamurthy M, Shkir M (2020) Fabrication of ON/OFF switching response based on n-Ni-doped MoO_3/ p-Si junction diodes using Ni-MoO_3 thin films as n-type layer prepared by JNS pyrolysis technique. Appl Phys A 126:216. https://doi.org/10.1007/s00339-020-3392-0

Balasubramani V, Chandrasekaran J, Manikandan V, Marnadu R, Vivek P, Balraju P (2020) Influence of rare earth doping concentrations on the properties of spin-coated V_2O_5 thin films and Cu/Nd-V_2O_5/n-Si Schottky barrier diodes. Inorg Chem Commun 119:108072. https://doi.org/10.1016/j.inoche.2020.108072

Ben Farhat L, Amami M, Hlil EK, Ben Hassen R (2010) Preparation, X-ray analysis and magnetic investigation of nano structured Co: Yb2O3. Mater Res Bull 45:1964–1968. https://doi.org/10.1016/j.materresbull.2010.08.007

Bhuvaneswari S, Seetha M, Chandrasekaran J, Marnadu R (2020) High photoresponsive p-Si/n-In_2O_3 junction diodes with low ideality factor prepared using closely packed octahedral structured In_2O_3 thin films. J Inorg Organomet Polym Mater. https://doi.org/10.1007/s10904-020-01663-x

Buyukbas-Ulusan A, Taşçıoğlu İ, Tataroğlu A, Yakuphanoğlu F, Altındal S (2019) A comparative study on the electrical and dielectric properties of Al/Cd-doped ZnO/p-Si structures. J Mater Sci: Mater Electron 30:12122–12129. https://doi.org/10.1007/s10854-019-01570-z

Caglar M, Ilican S, Caglar Y, Yakuphanoglu F (2009) Electrical conductivity and optical properties of ZnO nanostructured thin film. Appl Surf Sci 255:4491–4496. https://doi.org/10.1016/j.apsusc.2008.11.055

Casalino M, Sassi U, Goykhman I, Eiden A, Lidorikis E, Milana S, Ferrari AC (2017) Vertically illuminated, resonant cavity enhanced, graphene–silicon Schottky photodetectors. ACS Nano 11:10955–10963

Chen J, Lv J, Wang Q (2016) Electronic properties of Al/MoO3/p-InP enhanced Schottky barrier contacts. Thin Solid Films. https://doi.org/10.1016/j.tsf.2016.08.019

Desai SP (2018) Improved opto-electrical properties of spray deposited ytterbium doped cadmium oxide thin films. J Mater Sci: Mater Electron 29:14416–14426. https://doi.org/10.1007/s10854-018-9574-2

Di Bartolomeo A (2016) Graphene Schottky diodes: an experimental review of the rectifying graphene/semiconductor heterojunction. Phys Rep 606(8):1–58. https://doi.org/10.1016/j.physrep.2015.10.003

Di Bartolomeo A, Giubileo F, Luongo G, Iemmo L, Martucciello N, Niu G, Fraschke M, Skibitzki O, Schroeder T, Lupina G (2017) Tunable Schottky barrier and high responsivity in graphene/Sinanotip Optoelectronic device. Mater. https://doi.org/10.1088/2053-1583/4/1/015024

Di Bartolomeo A, Giubileo F, Grillo A, Luongo G, Iemmo L, Urban F, Lozzi L, Capista D, Nardone M, Passacantando M (2019) Bias tunable photocurrent in metal-insulator semiconductor heterostructures with photoresponse enhanced by carbon nanotubes. Nanomaterials 9(11):1598. https://doi.org/10.3390/nano9111598

Dogru Balbasi C, Terlemezoglu M, Gullu HH, Yildiz DE, Parlak M (2020) Electrical characterization of CdZnTe/Si diode structure. Appl Phys A 126:614. https://doi.org/10.1007/s00339-020-03772-3

Janardhanam V, Jyothi I, Kim Y, Lee SN, Yun HJ, Hong WK, Choi CJ (2020) 2020 Carrier conduction mechanisms of WSe2/p-type Ge epilayer heterojunction depending on the measurement temperature and applied bias. J Alloys Compd. https://doi.org/10.1016/j.jallcom.2020.155843

Jyothi V, Janardhanam JH, Kim HJ, Yun JC, Jeong H, Hong SN, Lee CJ (2016) Choi, Electrical and structural properties of Au/Yb Schottky contact on p-type GaN as a function of the annealing temperature. J Alloy Compds. https://doi.org/10.1016/j.jallcom.2016.07.292

Kahraman A, Karacali H, Yilmaz E (2020) Impact and origin of the oxide-interface traps in Al/Yb_2O_3/n-Si/Al on the electrical characteristics. J Alloy Compd 825:154171. https://doi.org/10.1016/j.jallcom.2020.154171

Katsuno T, Watanabe Y, Fujiwara H, Konishi M, Naruoka H, Morimoto J, Morino T, Endo T (2011) Analysis of surface morphology at leakage current sources of 4H–SiC Schottky barrier diodes. Appl Phys Lett 98:222111. https://doi.org/10.1063/1.3597413

Khanfar HK, Qasrawi AF, Zakarneh YA, Gasanly NM (2017) Design and applications of Yb/Ga_2Se_3/C schottky barriers. IEEE Sensors J. https://doi.org/10.1109/JSEN.2017.2702710

Lapa HE, Kökce A, Aldemir DA et al (2020) Effect of illumination on electrical parameters of Au/(P3DMTFT)/*n*-GaAs Schottky barrier diodes. Indian J Phys 94:1901–1908. https://doi.org/10.1007/s12648-019-01644-y

Lei L, Kuisheng Y, Xiyan Z, Ning Q, Hui L, Zhou Z (2012) Up-conversion luminescence properties of Yb3+ and Ho3+ co-doped Bi3.84W0.16O6.24 powder synthesized by hydrothermal method. J Rare Earths. https://doi.org/10.1016/S1002-0721(12)60185-9

Luongo G, Di Bartolomeo A, Giubileo F (2018) Carlos alvarado chavarin, and christian wenger, electronic properties of graphene/p-silicon schottky junction. J Phys D Appl Phys. https://doi.org/10.1088/1361-6463/aac562

Marikkannu S, Kashif M, Ayeshamariam A, Sethupathi N, Vidhya VS, Piraman S, Jayachandran M (2014) Studies on jet nebulizer pyrolysed indium oxide thin films. J Ovonic Res 10(4):115–125. https://doi.org/10.13140/2.1.5015.104

Marnadu R, Chandrasekaran J, Raja M, Balaji M, Balasubramani V (2018) Impact of Zr content on multiphase zirconium–tungsten oxide (Zr–WOx) films and its MIS structure of Cu/Zr–WOx/p-Si Schottky barrier diodes. J Mater Sci 29:2618–2627. https://doi.org/10.1007/s10854-017-8187-5

Marnadu R, Chandrasekaran J, Maruthamuthu S et al (2019) Ultra-high photoresponse with superiorly sensitive metal-insulator-semiconductor (MIS) structured diodes for UV photodetector application. Appl Surf Sci. https://doi.org/10.1016/j.apsusc.2019.02.214

Mohanraj K, Balasubramanian D, Chandrasekaran J (2018) Synthesis and characterization of ruthenium-doped CdO nanoparticle and its n-RuCdO/p-Si junction diode application. J Alloy Compd. https://doi.org/10.1016/j.jallcom.2018.11.264

Munikrishna Reddy Y, Lakshmi Narasappa T, Padman Suvarna R, Rajagopal Reddy V (2015) Analysis of electrical properties and carrier transport mechanisms of Ru/Ti/n-InP schottky diodes at room temperature. Int J New Tech Sci Eng 2(2):2349–2780

Muralidharan M, Sivakumar K, Sivaji K (2018) Structural, optical and magnetic properties of pure and Yb doped MnWO4 compounds. Mech Mater Sci Eng. https://doi.org/10.2412/mmse.96.6.507

Narmada A, Kathirvel P, Lakshmi M, Saravanakumar S, Marnadu R, Chandrasekaran J (2019) Jet nebuliser spray pyrolysed indium oxide and nickel doped indium oxide thin films for photodiode application. Optik. https://doi.org/10.1016/j.ijleo.2019.163701

Petroff P, Sheng TT, Sinha AK, Rozgonyi GA, Alexander FB (1973) Plasma processing for VLSI. J Appl Phys 44:2545

Prnová A, Bodišová K, Klement R, Migát M, Veteška P, Škrátek M, Bruneel E, Van Driessche I, Galusek D (2014) Preparation and characterization of Yb_2O_3–Al_2O_3 glasses by the Pechini sol–gel method combined with flame synthesis. Ceram Int 40:6179–6184. https://doi.org/10.1016/j.ceramint.2013.11.071

Puri N, Rohilla A, Chamoli SK, Mahapatro AK (2019) Effect of ytterbium oxide deposition on micro structural and electrical properties of thin tantalum foil. Mater Lett 253:67–70. https://doi.org/10.1016/j.matlet.2019.06.016

Qian L, Sun Y, Wu M, Xie D, Ding L, Shi G (2017) A solution-processed high performance phototransistor based on a perovskite composite with chemically modified graphenes. Adv Mater 29:1606175

Raj M, Joseph C, Subramanian M, Perumalsamy V, Elayappan V (2020) Superior photoresponse MIS Schottky barrier diodes with nanoporous: Sn-WO3 films for ultraviolet photodetector application. New J Chem. https://doi.org/10.1039/D0NJ00101E

Raja M, Chandrasekaran J, Balaji M, Kathirvel P, Marnadu R (2019) Influence of metal (M = Cd, In, and Sn) dopants on the properties of spin-coated WO3 thin films and fabrication of temperaturedependent heterojunction diodes. J Sol-Gel Sci Technol. https://doi.org/10.1007/s10971-019-05207-9

Rajagopal Reddy V, Dasaradha Rao L, Janardhanam V, Kang M-S, Choi C-J (2013) Electrical properties and interface states of rare-earth metal ytterbium schottky contacts to p-type InP. Mater Trans. https://doi.org/10.2320/matertrans.M2013281

Rajagopal Reddy V, Sri Silpa D, Janardhanam V (2015) Rapid thermal annealing effects on the electrical, structural and morphological properties of Yb/ p-type InP Schottky structure. Electron Matter Lett. https://doi.org/10.1007/s13391-014-1368-y

RajMohamed J, Amalraj L (2016) Effect of precursor concentration on physical properties of nebulized spray deposited In_2S_3 thin films. J Asian Ceramic Soc 4:357–366. https://doi.org/10.1016/j.jascer.2016.07.002

Riazimehr S, Kataria S, Bornemann R, Haringbolívar P, Ruiz FJG, Engström O, Lemme MC (2017) High photocurrent in gated graphene–silicon hybrid photodiodes. ACS Photonics 4:1506–1514

Sarath babu R, Narasimha murthy Y, Shkir M, AlFaify S (2020) In-depth analysis on Erbium co-doped CdO: Zn films deposited by nebulizer method for opto-electronic applications. J Mol Struct. https://doi.org/10.1016/j.molstruc.2020.128148

Scarel G, Svane A, Fanciulli M (2006) Scientific and technological issues related to rare earth oxides: an introduction. Top Appl Phys 106(2):1–14

Shkir M, Anis M, Shaikh SS, Hamdy MS, AlFaify S (2020) Impact of Se doping on optical and third order nonlinear optical properties of spray pyrolysis fabricated CdS thin films for optoelectronics. Appl Phys B 126:121. https://doi.org/10.1007/s00340-020-07472-x

Sonmezoglu S, Akın S (2012) High performance GaAs metal-insulator-semiconductor devices using TiO_2 as insulator layer. Curr Appl Phys 12:1372–1377. https://doi.org/10.1016/j.cap.2012.03.030

Suresh R, Ponnuswamy V, Mariappan R, Senthilkumar N (2014) Influence of substrate temperature on the properties of CeO2 thin films by simple nebulizer spraypyrolysis technique. Ceram Int 40:437–445. https://doi.org/10.1016/j.ceramint.2013.06.020

Tataroglu A, Altındal S (2008) Study on the frequency dependence of electrical and dielectric characteristics of Au/SnO2/n-Si (MIS) structures. Microelectron Eng 85:1866–1871. https://doi.org/10.1016/j.mee.2008.05.025

Terasaki N, Yamamoto N, Hattori M, Tanigaki N, Hiraga T, Ito K, Nakazato K (2009) Photosensor based on an FET utilizing a biocomponent of photosystem I for use in imaging devices. Langmuir 25:11969–11974

Thangaraju D, Marnadu R, Santhana V, Durairajan A, Kathirvel P, Chandrasekaran J, Jayakumar S, Valentec MA, Greenidgee DC (2020) Solvent influenced synthesis of single-phase SnS_2 nanosheets for solution-processed photodiode fabrication. Cryst Eng Comm 22:525–533. https://doi.org/10.1039/c9ce01417a

Uma M, Rajagopal Reddy V, Janardhanam V (2019) Chel-Jong Choi, Effect of rare-earth Pr6O11 insulating layer on the electrical properties of Au/n-GaN Schottky electrode and its chemical and structural characterization. J Mater Sci. https://doi.org/10.1007/s10854-019-02224-w

Vivek P, Chandrasekaran J, Marnadu R, Maruthamuthu S, Balasubramani V, Balraju P (2019a) Zirconia modified nanostructured MoO3 thin films deposited by spray pyrolysis technique for Cu/MoO3-ZrO2/p-Si structured Schottky barrier diode application. Optik 199:163351. https://doi.org/10.1016/j.ijleo.2019.163351

Vivek P, Chandrasekaran J, Marnadu R, Maruthamuthu S, Balasubramani V (2019b) Incorporation of Ba^{2+} ions on the properties of MoO3 thin films and fabrication of positive photo-response Cu/Ba–MoO3/p-Si structured diode. Superlattices Microstruct 133:106197. https://doi.org/10.1016/j.spmi.2019.106197

Vivek P, Chandrasekaran J, Marnadu R, Maruthamuthu S (2020) Fabrication of illumination-dependent Cu/p-Si schottky barrier diodes by sandwiching MoO_3 nanoplates as an interfacial layer via JNSP technique. J Electron Mater. https://doi.org/10.1007/s11664-020-08137-3

Zargouni S, El Whibi S, Tessarolo E, Rigon M, Martucci A, Ezzaouia H (2020a) Structural properties and defect related luminescence of Yb-doped NiO sol-gel thin films. Superlattices Microstruct 138:106361. https://doi.org/10.1016/j.spmi.2019.106361

Zargouni S, El Whibi S, Tessarolo E, Rigon M, Martucci A, Ezzaouia H (2020b) Structural properties and defect related luminescence of Yb-doped NiO sol-gel thin films. Superlattices Microstruct. https://doi.org/10.1016/j.spmi.2019.106361

Publisher's Note Springer Nature remains neutral with regard to jurisdictional claims in published maps and institutional affiliations.